Heme Binding to the Histidine-Rich Protein II from *Plasmodium falciparum*†

Eric L. Schneider‡ and Michael A. Marletta*,‡,§,||

Department of Chemistry, Department of Molecular and Cell Biology, and Division of Physical Biosciences, Lawrence Berkeley National Laboratory, University of California, Berkeley, Berkeley, California 94720-1460

Received July 6, 2004; Revised Manuscript Received October 5, 2004

ABSTRACT: The histidine-rich protein II (HRP II) from *Plasmodium falciparum* has been implicated in the formation of hemozoin, a detoxified, crystalline form of ferric protoporphyrin IX (Fe^{3+}-PPIX) produced by the parasite. Fe^{3+}-PPIX titrations coupled with quantitative amino acid analysis showed that HRP II binds 15 Fe^{3+}-PPIX molecules per 30 kDa monomer. Circular dichroism spectroscopy was used to probe the secondary structure of HRP II with and without bound Fe^{3+}-PPIX. These studies have revealed large changes in the secondary structure with Fe^{3+}-PPIX binding, changing from a random coil in the absence of Fe^{3+}-PPIX to a more ordered helical structure in the presence of Fe^{3+}-PPIX. The Fe^{3+}-PPIX-bound HRP II structure most closely resembles a 3_{10}-helix. Coincident with this structural change caused by Fe^{3+}-PPIX binding, the formation of an intermolecular disulfide bond occurs between HRP II monomers. In vitro pull-down assays show an interaction between monomers that is dependent on the presence of Fe^{3+}-PPIX. One model that best fits with the data reported here requires formation of 15 intermolecular bishistidyl ligated Fe^{3+}-PPIX molecules arranged in a head to head fashion, which would then allow for the formation of an intermolecular disulfide bond. The structure best able to accommodate these requirements is a 3_{10}-helix.

Malaria, a disease caused by the *Plasmodium* parasite, continues to be one of the most important diseases in the world, resulting in 300−500 million infections and more than 1 million deaths every year, as estimated by the WHO (*1*). Of the *Plasmodium* parasites that cause malaria in humans, *Plasmodium falciparum* has the highest mortality rate. Inside the human host, *P. falciparum* eventually invades red blood cells where it rapidly grows and multiplies, producing multiple copies of new parasites within 48 h. To support this growth, the parasite ingests up to 75% of the host hemoglobin into the food vacuole, which is then digested by a number of proteases (*2*, *3*). The resulting amino acids are then used as a source of nutrients by the parasite. In addition, the degradation of hemoglobin releases toxic free ferriprotoporphyrin IX (Fe^{3+}-PPIX)[1] into the parasite food vacuole (*4*). Because of the toxic effect Fe^{3+}-PPIX has on the parasite (*5*, *6*), it is imperative for *P. falciparum* to detoxify free Fe^{3+}-PPIX which it accomplishes in a unique way by forming hemozoin, an insoluble, crystalline form of Fe^{3+}-PPIX. The structure of hemozoin involves the dimerization of Fe^{3+}-PPIX molecules through reciprocal iron−carboxylate ligation. Hydrogen bonding occurs between the free carboxylates of separate dimers to form a chain of dimers (*7*).

The need for a variety of effective antimalarials has increased dramatically because of resistance to the most common and inexpensive drug, chloroquine (*8*). Since humans do not rely on hemozoin formation for Fe^{3+}-PPIX detoxification, this mechanism for Fe^{3+}-PPIX disposal is an ideal target for antimalarial drug development. The exact mechanism for hemozoin formation by *P. falciparum* is still under debate (*9*), with reports demonstrating hemozoin formation through self-catalysis (*10*), in the presence of histidine-rich proteins (*11*) or lipids (*12*, *13*), and through combinations of these factors (*10*, *13*−*15*).

The histidine-rich proteins are the only proteins to date that continue to be implicated in hemozoin formation. Studies by Choi et al. have shown that HRP II directly interacts with multiple Fe^{3+}-PPIX molecules, increasing support for its role in Fe^{3+}-PPIX detoxification (*16*). However, studies on parasites lacking HRP II and HRP III maintain the ability to produce hemozoin, indicating that these proteins, although capable, are not essential for hemozoin formation. This study at the same time does not rule out the participation of other histidine-rich proteins. Akompong et al. have recently investigated the subcellular localization of HRP II and found that 97% is exported to the erythrocyte cytosol with the remaining 3% located in the parasite food vacuole, suggesting that the main function of HRP II is not hemozoin formation (*17*). However, the population located in the food vacuole may still play an important role in hemozoin formation, while the cytosolic HRP II may be involved in Fe^{3+}-PPIX scavanging.

† This work was supported by the Burroughs-Wellcome Fund, New Initiatives in Malaria Research.

* To whom correspondence should be addressed at the Department of Chemistry, University of California, Berkeley, 211 Lewis Hall, Berkeley, CA 94720-1460. Phone: (510) 643-9325. Fax: (510) 643-9388. E-mail: marletta@berkeley.edu.

‡ Department of Chemistry, UCB.

§ Department of Molecular and Cell Biology, UCB.

|| Division of Physical Biosciences, LBNL.

[1] Abbreviations: Fe^{3+}-PPIX, ferric protoporphyrin IX; HRP II, histidine-rich protein II; HRP II(C274S), histidine-rich protein II Cys274 to Ser mutant; HEPES, 4-(2-hydroxyethyl)-1-piperazineethanesulfonic acid; CD, circular dichroism; PAGE, polyacrylamide gel electrophoresis; MMTS, methyl methanethiosulfonate; DTT, dithiothreitol.

10.1021/bi048570p CCC: $30.25
Published on Web 12/24/2004

HRP II is a 30 kDa protein composed of two repeats (His-His-Ala-His-His-Ala-Ala-Asp-Ala and His-His-Ala-Ala-Asp) that comprise nearly 85% of the amino acids in the protein sequence (*18*, *19*). Previous studies on Fe^{3+}-PPIX binding by HRP II have found it to bind multiple Fe^{3+}-PPIX molecules per monomer (*11*, *16*, *20*). These Fe^{3+}-PPIX molecules are bound as low-spin, ferric Fe^{3+}-PPIX through bishistidyl ligation (*16*). Because the ability to ligate a large number of Fe^{3+}-PPIX molecules has been found in only a few other proteins (*21*, *22*), understanding how HRP II is able to accommodate these Fe^{3+}-PPIX may lead to a greater understanding of its function. In this report we have investigated the structural requirements necessary for Fe^{3+}-PPIX binding by HRP II using various biochemical techniques. Binding of Fe^{3+}-PPIX by HRP II causes large changes in the protein secondary structure changing from a random coil in the absence of Fe^{3+}-PPIX to a structure that fits the circular dichroism signature of a 3_{10}-helix when Fe^{3+}-PPIX is bound. Along with this gross secondary structure change, we have detected an interaction between HRP II monomers dependent on Fe^{3+}-PPIX binding as well as the formation of an intermolecular disulfide bond. These findings allow us to speculate on the structure of the HRP II−Fe^{3+}-PPIX complex.

MATERIALS AND METHODS

Materials. Escherichia coli competent cells were purchased from Novagen. IPTG was purchased from Promega. Novex 10−20% Tris−glycine gels were purchased from Invitrogen. All restriction enzymes were purchased from New England Biolabs. PCR primers were purchased from Gibco/Life Technologies. Anti-myc antibody was purchased from Roche. Anti-biotin antibody was purchased from Zymed. All other chemicals were purchased from Sigma-Aldrich unless otherwise noted.

General Methods. Quantitative amino acid analysis was performed by the Protein Chemistry Laboratory at Texas A&M University using a Hewlett-Packard AminoQuant II system to verify the results of the biuret assay. Fe^{3+}-PPIX titrations were performed, as previously described (*16*), using a Cary 300 spectrophotometer at 25 °C. All samples of Fe^{3+}-PPIX were made from stock solutions of hemin chloride in 100 mM NaOH.

Construction of the c-myc-HRP II Expression Vector. A c-myc epitope tag (amino acid sequence EQKLISEEDL) was inserted N-terminal to HRP II. The c-myc-HRP II expression vector was made by PCR using a sense primer that abolished the existing ATG start codon and introduced the underlined codons for the c-myc tag along with a new ATG start codon inside a unique *Nco*I site (5′-GAGGAGCCATGGGA-GAGCAGAAACTCATCTCTGAAGAAGATCTGGGAG-CAAAAAATGCAAAAGGACTTAATTTA-3′). The antisense primer introduced a unique *Hin*dIII site (5′-TGCTAGC-CAAGCTTAATGGCGTAGG-3′). PCR of pET3d-HRP II yielded an 890-bp product. The procedures described for the handling of the PCR product during the construction of pET21d-HRP II(C274S) (*37*) were followed to yield pET21d-c-myc-HRP II. The plasmid sequence was confirmed by the UC Berkeley DNA sequencing facility.

Expression and Purification of HRP II, c-myc-HRP II, and HRP II(C274S). Recombinant HRP II was expressed using the appropriate plasmid [pET21d-HRP II (*37*) for wild type, pET21d-c-myc-HRP II for c-myc-HRP II, or pET21d-SerHRP II for HRP II(C274S) (*37*)] in BL21(DE3) pLysS competent cells. Expression was induced by addition of 0.5 μM isopropyl β-D-thiogalactopyranoside (IPTG) at an OD_{600} of 0.6−0.8 as previously described. All expressed proteins were purified using nickel chelate chromatography as previously described (*11*, *16*). Western blotting with an anti-c-myc antibody was used to confirm that the purified c-myc-labeled HRP II contained the c-myc tag.

The purified HRP II and c-myc-HRP II were reduced by reaction with 10 mM dithiothreitol (DTT) for 1 h. Excess DTT was removed using a PD-10 desalting column (Pharmacia). The protein concentrations were determined by the biuret assay according to Gornall et al. (*23*). A 10 mM BSA protein solution in 100 mM HEPES, pH 7.0, was used to create a standard curve. [The standard or sample (40 μL) in 100 mM HEPES, pH 7.0, was combined with 160 μL of the biuret reagent (6 mM $CuSO_4$, 21 mM sodium potassium tartrate, 750 mM NaOH in H_2O) in triplicate.] The samples were incubated with shaking for 30 min at 25 °C. The A_{550} was read on a Molecular Devices Thermomax microplate reader.

Circular Dichroism Studies of HRP II. HRP II (5.7 μM) was combined with Fe^{3+}-PPIX at 17, 34, 51, 68, and 85 μM, respectively, in 20 mM potassium phosphate, pH 7.0. An identical sample was also prepared with no Fe^{3+}-PPIX. The samples were incubated at 25 °C for 15 min. The circular dichroism spectrum of each sample was measured using a 1 mm path length cell at 25 °C on a Jasco J-810 CD spectrophotometer.

Disulfide Bond Formation between HRP II Monomers. A 40 μL solution of purified and reduced HRP II (17.6 μM) was incubated with saturating levels of Fe^{3+}-PPIX (261 μM Fe^{3+}-PPIX) or no Fe^{3+}-PPIX for 30 min at 25 °C in 10 mM ammonium acetate, pH 7.0. Samples were run on Novex 10−20% Tris−glycine gels under native conditions and stained with Coomassie blue R-250. Thiol modification by methyl methanethiosulfonate (MMTS) was achieved by incubating 100 μL of reduced, purified HRP II (351 μM) with 1.4 mM MMTS in 10 mM ammonium acetate, pH 7.0, at 25 °C for 1 h. A 2 μL aliquot of this solution was diluted to 40 μL (to 17.6 μM) prior to following the procedure above.

A 50 μL solution was prepared containing 17.6 μM HRP II(C274S) with saturating levels of Fe^{3+}-PPIX (261 μM Fe^{3+}-PPIX) or no Fe^{3+}-PPIX in 100 mM HEPES, pH 7.0. After 90 min at 25 °C, the samples were run on Novex 10−20% Tris−glycine gels under nonreducing, denaturing conditions and stained with Coomassie blue R-250.

A 10 μL solution was prepared containing 20 μM HRP II with 280 μM Fe^{3+}-PPIX, 280 μM iron citrate, or no additions in 100 mM HEPES, pH 7.0. After 90 min, 1 mM iodoacetamide was added to the solution to react with any free cysteines. Samples were run on Novex 10−20% Tris−glycine gels under nonreducing, denaturing conditions and stained with Coomassie blue R-250.

Biotinylation of HRP II. A 1 mL solution of 18 μM HRP II was mixed with 1 mM dithiothreitol (DTT) at 25 °C for 1 h to ensure that all cysteine residues were reduced. The DTT was removed using a PD-10 desalting column (Pharmacia) by elution with 1.5 mL of 100 mM HEPES, pH 7.0. The HRP II solution was eluted directly into a microcentri-

fuge tube containing 2 mg of EZ-link PEO-maleimide-activated biotin (Pierce) to give a final concentration of 2.5 mM biotin. The reaction proceeded overnight at 25 °C. The free EZ-link PEO-maleimide-activated biotin was removed from the biotinylated HRP II with a PD-10 desalting column. Biotinylation of HRP II was verified by Western blotting using an anti-biotin antibody.

Pull-Down Experiments with c-myc-HRP II and Biotinylated HRP II. ImmunoPure immobilized streptavidin (Pierce) was blocked with 5% nonfat dry milk in pull-down buffer (20 mM sodium phosphate, 500 mM NaCl, pH 7.5) overnight at 4 °C on a rotating platform. The resin was then washed three times with 1 mL of the pull-down buffer. Samples containing biotinylated HRP II, c-myc HRP II, and Fe^{3+}-PPIX were prepared as indicated in the results. After 30 min at 25 °C, each sample (100 μL) was added to 20 μL of washed resin and placed on a rotating platform overnight at 4 °C. The samples were spun at 1000 rpm in a microcentrifuge, and the sample was decanted from the pelleted resin. The resin was washed three times with 1 mL of the pull-down buffer, and the sample for analysis was eluted by addition of 50 μL of 6× SDS gel loading buffer (0.35 M Tris-HCl, 3 mL of glycerol, 1 g of SDS, and 1.2 mg of bromophenol blue in 10 mL total volume).

Western Blot Analysis. Samples were run on Novex 10−20% Tris−glycine gels (Invitrogen) and transferred to Protran nitrocellulose membranes (Schleicher and Schuell). The membranes were blocked with 5% nonfat dry milk in PBS−Tween buffer (phosphate-buffered saline, pH 7.4, with 0.01% Tween 20) for 1 h. Labeled HRP II was detected by incubation with mouse monoclonal anti-biotin or mouse monoclonal anti-c-myc primary antibody for 1 h, followed by incubation with a horseradish peroxidase-conjugated goat anti-mouse secondary antibody for 1 h. An ECL Western blotting analysis detection system (Amersham Biosciences) was used to visualize the bands.

RESULTS

Spectroscopic Quantification of the Fe^{3+}-PPIX Binding Sites on HRP II and HRP II(C274S). Previously we used the bicinchoninic acid (BCA) assay to determine the concentration of HRP II and concluded that HRP II bound 50 equivalents of Fe^{3+}-PPIX (*16*). Continued studies demonstrated that this assay underestimated the concentration of HRP II. The biuret assay was compared to quantitative amino acid analysis (QAA) and provided convincing evidence that the biuret assay was accurate. Spectroscopic Fe^{3+}-PPIX titration experiments subsequently determined an HRP II:Fe^{3+}-PPIX binding stoichiometry of 15 Fe^{3+}-PPIX/HRP II (Figure 1A). Similarly, HRP II(C274S) was found to have a nearly identical Fe^{3+}-PPIX binding stoichiometry of 16 Fe^{3+}-PPIX/HRP II(C274S) (Figure 1B). The K_d values for Fe^{3+}-PPIX binding were found to be 0.34 and 0.16 μM for HRP II and HRP II(C274S), respectively. Both of the proteins showed similar cooperative Fe^{3+}-PPIX binding with Hill coefficients of 2.3 for HRP II and 2.5 for HRP II(C274S).

Circular Dichroism Studies of HRP II and HRP II−Fe^{3+}-PPIX. The CD spectra for HRP II and HRP II as a function of bound Fe^{3+}-PPIX are shown in Figure 2. HRP II has a CD spectrum with a negative peak at 197 nm, indicative of random coil secondary structure. Furthermore, the CD spectrum does not change with increases in temperature (data not shown). The HRP II−Fe^{3+}-PPIX complex with saturating Fe^{3+}-PPIX (15:1) has negative peaks at 207 and 222 nm, with a 222:207 nm ratio of 0.6. The characteristics of this spectrum are indicative of a helical-type structure, most closely resembling a 3_{10}-helix-type CD spectrum (*24*). The HRP II−Fe^{3+}-PPIX complexes at subsaturating Fe^{3+}-PPIX concentrations appear to have secondary structures that are a mixture of random coil and helix. At 9 Fe^{3+}-PPIX equivalents per HRP II monomer and higher, the CD spectra do not change further.

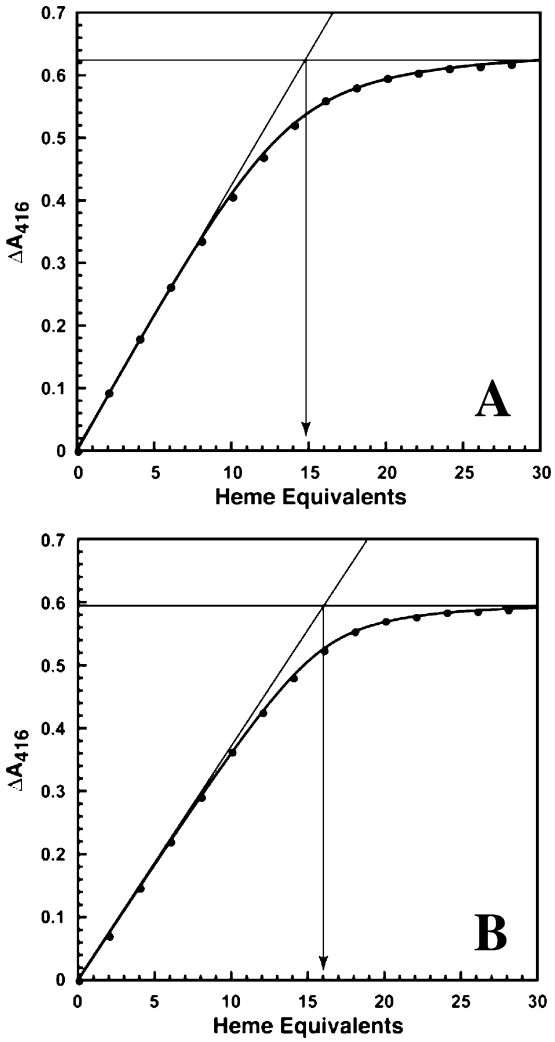

FIGURE 1: HRP II and HRP II(C274S) Fe^{3+}-PPIX binding plots. A plot of ΔA_{416} versus the Fe^{3+}-PPIX concentration from the difference absorption spectra obtained during Fe^{3+}-PPIX titrations of HRP II (panel A) and HRP II(C274S) (panel B) to give the Fe^{3+}-PPIX binding curves (●, both panels). These binding curves were fit by the equation described previously (*16*) and indicated that HRP II bound 15 Fe^{3+}-PPIX at saturation (panel A, solid curve) and HRP II(C274S) bound 16 Fe^{3+}-PPIX at saturation (panel B, solid curve). The intersection of the two straight lines drawn from the initial binding slope and the saturation point also demonstrate the Fe^{3+}-PPIX equivalents bound at saturation.

Intermolecular Disulfide Bond Formation. HRP II and the HRP II−Fe^{3+}-PPIX complex (15:1) were analyzed using native PAGE gels. As shown in Figure 3, the HRP II−Fe^{3+}-PPIX complex (lane 2) runs different than HRP II (lane 1). Compared to lane 1, the lower band is significantly broader, and a new band appears above it that is only faintly observed

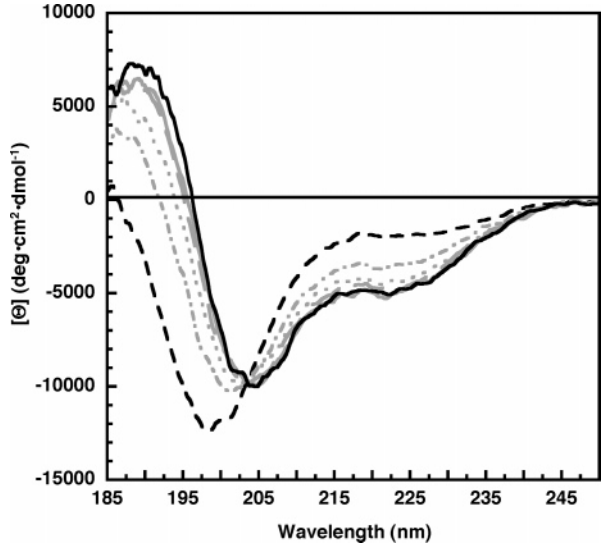

FIGURE 2: Circular dichroism spectra of HRP II. Samples contained HRP II and no Fe^{3+}-PPIX (black dashed line), 3 Fe^{3+}-PPIX equivalents (gray dash−dot line), 6 Fe^{3+}-PPIX equivalents (gray dotted line), 9 Fe^{3+}-PPIX equivalents (gray, large dashed line), 12 Fe^{3+}-PPIX equivalents (gray solid line), or 15 Fe^{3+}-PPIX equivalents (black solid line).

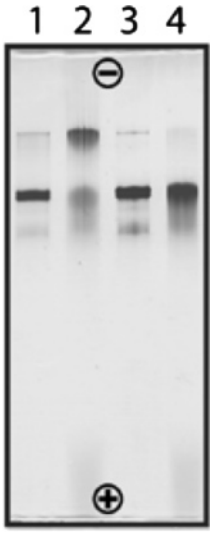

FIGURE 3: Native PAGE results reveal the formation of an intramolecular disulfide bond between HRP II monomers. Lanes: 1, reduced HRP II; 2, HRP II with Fe^{3+}-PPIX; 3, reduced and MMTS-treated HRP II; 4, reduced and MMTS-treated HRP II with Fe^{3+}-PPIX. When HRP II is incubated with Fe^{3+}-PPIX prior to electrophoresis, it migrates as a larger species. However, when HRP II is incubated with MMTS prior to incubation with Fe^{3+}-PPIX, mobility is unaffected. Heme dissociates during the running of the gel and can be seen as a broad band at the bottom of lanes 2 and 4. The positive and negative signs indicate the cathode and anode, respectively.

in the reduced sample. S-Methylation of the cysteine in HRP II with MMTS prior to addition of saturating Fe^{3+}-PPIX (lane 4) gave a result similar to HRP II samples containing no Fe^{3+}-PPIX (lane 1). Incubation of HRP II with MMTS prior to running on a native PAGE gel resulted in no electrophoretic mobility change in the absence of Fe^{3+}-PPIX (lane 3). When the HRP II−Fe^{3+}-PPIX complex was incubated with DTT prior to SDS−PAGE, HRP II from the complex also migrated similar to HRP II in the absence of Fe^{3+}-PPIX (data not shown). The minor bands in lanes 1, 3, and 4 running similarly to the upper band in lane 2 are likely due

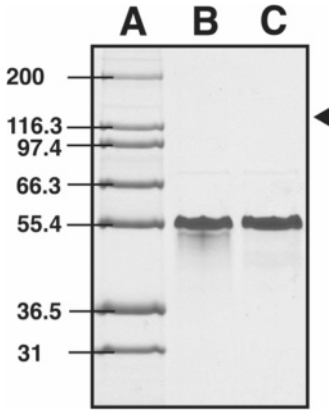

FIGURE 4: Nonreducing SDS−PAGE of HRP II(C274S) with Fe^{3+}-PPIX. Lanes: A, Mark 12 molecular mass standards; B, HRP II-(C274S) with Fe^{3+}-PPIX; C, HRPII(C274S). Incubation of HRPII-(C274S) with Fe^{3+}-PPIX has no effect on the migration of the protein on nonreducing SDS−PAGE. HRP II(C274S) migrates at ∼55 kDa with and without Fe^{3+}-PPIX present. The aberrant migration is similar to that seen for HRP II.

to disulfides formed prior to the experiment and MMTS labeling. The origin of the lowest band (most clearly seen in lanes 1 and 3) is unknown. Fe^{3+}-PPIX addition clearly broadens all of the protein bands. The Fe^{3+}-PPIX bound to HRP II prior to loading on the native PAGE gel can be seen near the bottom of lanes 2 and 3, indicating that Fe^{3+}-PPIX dissociates from HRP II under the conditions of native PAGE gel electrophoresis.

Analysis of HRP II(C274S) and the HRP II(C274S)−Fe^{3+}-PPIX complex by nonreducing SDS−PAGE shows Fe^{3+}-PPIX to have no effect on the mobility of this mutant (Figure 4). HRP II(C274S) has the same mobility in the presence of Fe^{3+}-PPIX (lane B) as it does in the absence of Fe^{3+}-PPIX (lane C).

In the presence of iron citrate, when run on a nonreducing SDS−PAGE gel, a small fraction of HRP II runs at a higher molecular mass (Figure 5, lane C), very similar to HRP II alone (Figure 5, lane B). The effect of Fe^{3+}-PPIX on HRP II was run again for comparison (Figure 5, lane D). The nonreducing, denaturing gel with molecular mass standards reveals that the high molecular mass species (∼116 kDa) is approximately twice the size of the low molecular mass species (∼55 kDa). Although HRP II runs as a 55 kDa species on SDS−PAGE, mass spectral analysis has shown it to have a molecular mass of 29160 Da as predicted. The reason for the aberrant mass on SDS−PAGE is unknown.

Interaction of HRP II Monomers Induced by Fe^{3+}-PPIX Binding. In vitro pull-down studies were performed to determine if the binding of Fe^{3+}-PPIX by HRP II led to an interaction between monomers. The results of the pull-down experiments with c-myc-HRP II and biotinylated HRP II are shown in Figure 6. When c-myc-HRP II was incubated with streptavidin resin in the presence of Fe^{3+}-PPIX, the c-myc-HRP II was not seen in the elution sample, indicating that the c-myc-HRP II−Fe^{3+}-PPIX complex does not bind to the streptavidin resin (Figure 6, lane A). Biotinylated HRP II in the presence of Fe^{3+}-PPIX was also incubated with the streptavidin resin and found in the elution sample as expected (Figure 6, lane B). Figure 6, lane B, also demonstrates the specificity of the antibodies used in the Western blots. The anti-c-myc antibody (Figure 6, lane B, lower panel) shows

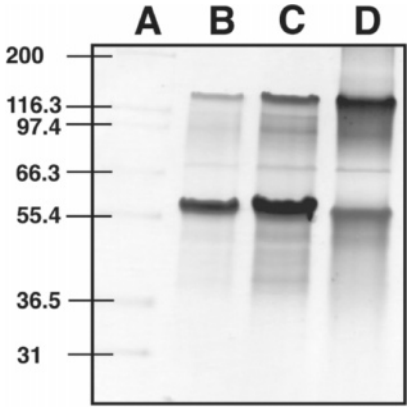

FIGURE 5: HRP II reaction with iron citrate run on nonreducing SDS−PAGE. Lanes: A, Mark 12 molecular mass standard (Invitrogen); B, reduced HRP II; C, HRP II with iron citrate; D, HRP II with Fe^{3+}-PPIX. Incubation of HRP II with iron citrate prior to electrophoresis on a nonreducing SDS−PAGE gel causes less of the HRP II to migrate as a higher molecular mass species than when HRP II is in the presence of Fe^{3+}-PPIX. The proportion of HRP II that migrates as a higher molecular mass species when incubated with iron citrate is similar to reduced HRP II alone. The molecular mass markers indicate that the larger species is approximately double the size of the smaller species. As seen previously, the HRP II monomer runs higher on SDS−PAGE (~60 kDa) than its actual molecular mass (29 kDa).

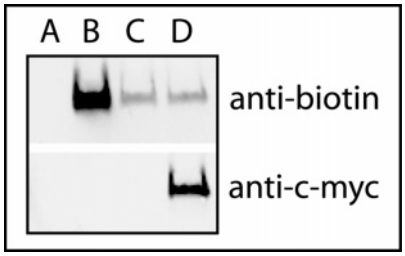

FIGURE 6: HRP II in vitro pull-down assay. Western blotting was performed on each elution sample using antibodies to c-myc and biotin. All samples were the elute from the streptavidin resin. Lane A is from the c-myc-HRP II−Fe^{3+}-PPIX sample, lane B is the biotinylated HRP II−Fe^{3+}-PPIX sample, lane C is a 5:1 c-myc-HRP II:biotinylated HRP II sample, and lane D is a 5:1 c-myc-HRP II:biotinylated HRP II sample with Fe^{3+}-PPIX. The presence of biotinylated HRP II is seen in lanes B−D. The presence of c-myc-HRP II is seen only in lane D, indicating an interaction between the HRP II monomers during Fe^{3+}-PPIX binding.

no cross-reactivity with the biotinylated HRP II. When c-myc-HRP II and biotinylated HRP II were combined at a 5:1 ratio and incubated with the streptavidin resin in the absence of Fe^{3+}-PPIX, only the biotinylated HRP II was eluted from the washed resin, indicating that c-myc-HRP II does not bind to the resin in the absence of Fe^{3+}-PPIX or interact with biotinylated HRP II (Figure 6, lane C). Addition of saturating Fe^{3+}-PPIX to the 5:1 c-myc-HRP II:biotinylated HRP II sample before incubation with the streptavidin resin resulted in the presence of both c-myc-HRP II and biotinylated HRP II in the elution sample, indicating an interaction between the c-myc-HRP II and biotinylated HRP II in the presence of Fe^{3+}-PPIX (Figure 6, lane D).

DISCUSSION

Fe^{3+}-PPIX Binding by HRP II. It became clear during the course of these studies that the measurement of HRP II concentration in solution was not straightforward. Further studies into the quantification of HRP II using the BCA method have revealed that it can underestimate the protein concentration by greater than 3-fold. The biuret assay was found to give a more precise, reproducible value for HRP II concentration. Comparison to quantitative amino acid analysis results indicated that no correction factor was needed for the biuret assay.

Because earlier studies have shown that HRP II heme binding is similar at pH 7.0 and 5.5, the pH of the parasite food vacuole, all experiments were performed at pH 7.0 in order to avoid heme insolubility and other precipitation issues (*16*). Fe^{3+}-PPIX titrations gave a stoichiometry of 15 Fe^{3+}-PPIX per monomer at saturation (Figure 1A). A similar Fe^{3+}-PPIX binding stoichiometry of 16 Fe^{3+}-PPIX per monomer was determined for the HRP II(C274S) mutant, indicating similar Fe^{3+}-PPIX binding properties. Other investigators have reported finding between 17 and 18 Fe^{3+}-PPIX bound at saturation, similar to what we report here (*11*, *20*). Although the number of histidine residues in HRP II (99 histidine) and the bishistidyl ligation of Fe^{3+}-PPIX by HRP II could lead to 50 bound Fe^{3+}-PPIX per HRP II if all His residues were involved in Fe^{3+}-PPIX ligation, it is clear that only a subset of 30 His residues is involved. The K_d values for Fe^{3+}-PPIX binding for both HRP II (0.34 μM) and the mutant (0.16 μM) were found to be similar to values already reported (*20*). The Fe^{3+}-PPIX binding data also revealed Hill coefficients indicating similar cooperativity in Fe^{3+}-PPIX binding by both HRP II and the mutant.

Detection of Fe^{3+}-PPIX Binding Dependent HRP II Structural Changes by Circular Dichroism. CD spectrum of HRP II (Figure 2, dashed line) is indicative of a random coil structure as defined by Fasman (*25*). However, as Fe^{3+}-PPIX is titrated into a solution of HRP II, the CD spectrum and, accordingly, the secondary structure change dramatically. Binding of Fe^{3+}-PPIX changes the CD spectrum of HRP II from the signature spectrum of a random coil to the spectrum indicative of a helical structure (Figure 2, solid line), with intermediate spectra appearing as a mixture of the initial and final spectra (Figure 2, various gray lines). This change in the CD spectrum indicates a large change in the overall secondary structure, induced by Fe^{3+}-PPIX binding to HRP II, to a protein with helical character.

The CD spectrum of the saturated HRP II−Fe^{3+}-PPIX complex does not exactly match that of a typical α-helix secondary structure as reported by Fasman, which has negative peaks at 207 and 222 nm with a 222:207 nm ratio of ~1 (*25*). The 222:207 nm ratio for the HRP II−Fe^{3+}-PPIX complex is approximately 0.6. Toniolo et al. have reported a ratio similar to this (222:207 nm = 0.4) for a peptide 3_{10}-helix (*24*). However, the assignment of a 222:207 nm ratio of 0.4 to a 3_{10}-helix is controversial, with suggestions that observation of this ratio alone is not enough to definitively assign a 3_{10}-helix secondary structure (*26*). When modeled as a 3_{10}-helix, the common repeats found throughout the protein (HHAHHAADA at the N-terminus and HHAADA at the C-terminus) place histidine residues at every third and/or every sixth position. Modeling of the entire sequence places 92 of the 99 histidine residues along two edges of the 3_{10}-helix, as shown in Figure 7A,B, whereas modeling the sequence as an α-helix does not result in an alignment of His residues (Figure 7C). Because previous studies have shown HRP II to bind Fe^{3+}-PPIX through bishistidyl ligation, the alignment of histidine residues

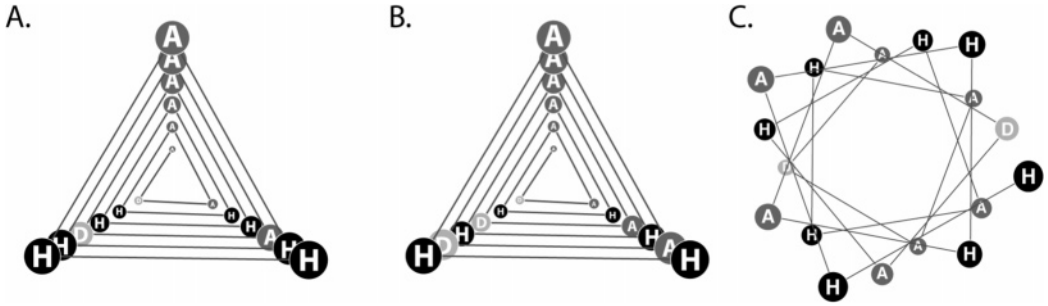

FIGURE 7: HRP II repeats modeled as 3_{10}- and α-helices. (A) Two repeats of His-His-Ala-His-His-Ala-Ala-Asp-Ala modeled as a 3_{10}-helix. (B) Three repeats of His-His-Ala-Ala-Asp-Ala modeled as a 3_{10}-helix. (C) Two repeats of His-His-Ala-His-His-Ala-Ala-Asp-Ala modeled as an α-helix. For all models, histidine is in black (H), alanine is in dark gray (A), and aspartate is in light gray (D). In models A and B, the histidine residues align two corners of the model, with alanine residues aligning along the third corner. In model A the repeat allows for histidine residues *N* and *N* + 3 to align next to each other, whereas the sequence of model B places one residue between every histidine along the same axis. In model C, the histidine residues are found all along the perimeter of the helix.

achieved with the 3_{10}-helix is very attractive. Other investigators have predicted the secondary structure of HRP II to be 3_{10}-helical because the repetitive nature of the sequence is based on groups of three (*19*, *27*). Although 3_{10}-helices are commonly found in proteins, they typically exist as short sequences of three to four residues, many times associated with the N- or C-termini of α-helices (*28*−*30*). The length of the 3_{10}-helix formed by HRP II could be quite long; however, we cannot estimate the length of the helix that forms upon Fe^{3+}-PPIX binding. It could run the length of the protein or could be in short stretches of the sequence where Fe^{3+}-PPIX is bound.

Interaction between HRP II Monomers. In the presence of saturating Fe^{3+}-PPIX (15:1 Fe^{3+}-PPIX:HRP II), HRP II was found to form a higher molecular mass species, as seen by native PAGE (Figure 3, lane 2). Nonreducing SDS−PAGE indicated that this higher molecular mass species was approximately double the mass of HRP II in the absence of Fe^{3+}-PPIX. Formation of this higher molecular mass species, however, was not observed when the lone cysteine in the protein sequence was blocked by the formation of an *S*-methyl disulfide with MMTS (Figure 3, lane 1) or mutated to a serine (Figure 4, lane B). Furthermore, when DTT was added to the sample prior to native PAGE analysis (data not shown), the higher molecular mass species was not observed.

All of these results indicate the formation of a disulfide bond between two monomers of HRP II induced by the presence of Fe^{3+}-PPIX. Although this result could potentially be explained by an oxidative environment produced by the presence of Fe^{3+}-PPIX, results using ferric citrate as an oxidant suggest that it is not a simple oxidation. In the presence of ferric citrate, the formation of an intermolecular disulfide was observed to a much lesser extent than with Fe^{3+}-PPIX (Figure 5). This result implies that the structural changes necessary for Fe^{3+}-PPIX binding are also required for disulfide bond formation. One interpretation is that the structural changes bring two HRP II monomers within close proximity, thereby facilitating disulfide bond formation.

To further explore the possibility of a Fe^{3+}-PPIX-induced interaction between HRP II monomers, in vitro pull-down studies were performed using HRP II modified with two separately identifiable tags, a c-myc epitope tag and cysteine-reactive biotin. When various combinations of the tagged HRP II constructs were incubated with and without Fe^{3+}-PPIX in the presence of streptavidin resin as shown in Figure 6, the biotinylated HRP II was found to bind to the resin as expected. The c-myc-tagged HRP II was only found in the eluent when Fe^{3+}-PPIX and biotinylated HRP II were also present in the initial sample (Figure 6, lane D). Because c-myc-tagged HRP II did not bind to the streptavidin under any other conditions, this result showed an interaction between the two labeled HRP II monomers that is dependent upon Fe^{3+}-PPIX. Because both of the labeled HRP II monomers have blocked cysteines in these pull-down experiments, this interaction is independent of the disulfide formation shown above. However, this result strengthens the hypothesis that Fe^{3+}-PPIX binding by HRP II brings two monomers within close proximity. Binding of Fe^{3+}-PPIX by HRP II causes an interaction between monomers along with the formation of an intermolecular disulfide bond.

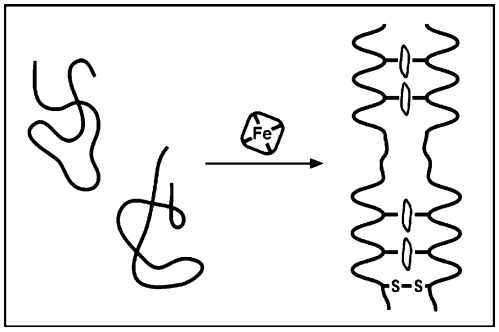

FIGURE 8: Summary of the structural changes of HRP II upon Fe^{3+}-PPIX binding.

Model of Conformational Changes Induced upon Fe^{3+}-PPIX Binding. Characterization of these conformational changes upon Fe^{3+}-PPIX binding allows for speculation about the structure necessary for HRP II to bind 15 Fe^{3+}-PPIX molecules through bishistidyl ligation. The results presented here indicate that Fe^{3+}-PPIX binding induces secondary structural changes resulting in a 3_{10}-helix. Along with this secondary structural change Fe^{3+}-PPIX binding also leads to an interaction between HRP II monomers and the formation of an intermolecular disulfide bond between monomers.

The simplest model that can account for these Fe^{3+}-PPIX binding induced structural changes to HRP II is summarized in Figure 8. In this model, each HRP II monomer contributes one of the two histidine residues necessary for Fe^{3+}-PPIX binding, resulting in a HRP II dimer. This ligation matches up the histidine faces, created by the 3_{10}-helical secondary structure, at the dimer interface. This model allows for two

possible orientations of the HRP II monomers relative to each other (parallel, C-terminus next to C-terminus, or antiparallel, C-terminus next to N-terminus). However, formation of a disulfide bond between the cysteines located near the C-termini requires the monomers to orient in a parallel fashion. These studies cannot completely rule out the possibility of an α-helical secondary structure; however, alignment of the histidine residues in a 3_{10}-helix allows for the creation of 15 Fe^{3+}-PPIX binding sites more readily than a similar dimer of α-helices. Although the 3_{10}-helix is inherently less stable than the α-helix, 3_{10}-helices are found in numerous proteins at lengths of up to 10 residues (*31*). A 13-residue peptide was recently found to adopt a 3_{10}-helical secondary structure in solution (*32*). Additionally, the residues Ala, Asp, and His, which comprise a majority of the HRP II sequence, are overrepresented in 3_{10}-helices, potentially predisposing the secondary structure (*30*, *31*). Fe^{3+}-PPIX binding may provide the necessary stabilization for 3_{10}-helix formation.

This model creates a histidine/Fe^{3+}-PPIX core while leaving the aligned alanine residues exposed to solution, an energetically unfavorable situation. An adjustment to this model would place the alanine face along with one of the histidine faces at the dimer interface. The alignment of only one histidine face from each monomer would still provide the 30 histidine residues necessary for Fe^{3+}-PPIX binding while also burying the hydrophobic alanine residues and potentially adding some stability to the overall structure through these hydrophobic interactions. Alternatively, the exposed alanine faces could interact to create higher order multimers, a possibility not prohibited by the data presented here.

Exactly how the dimer forms is a question that remains unanswered. Short α-helical peptides containing histidine have been successfully designed to bind various heme molecules through bishistidyl ligation with two monomers, each contributing one histidine ligand, similar to our proposal for HRP II (*33*−*36*). Heme binding by some of these designed peptides results in a secondary structure transition from random coils to α-helices (*34*−*36*). Assembly into dimers is also seen upon heme binding (*35*). However, these peptides are designed with limited heme binding capacity (one or two hemes per dimer), making the dimer assembly and secondary structural changes less complex than what is necessary for the significantly larger HRP II. If the initial Fe^{3+}-PPIX binding event, binding of the first Fe^{3+}-PPIX equivalent, occurs between random histidine residues of the two HRP II monomers, then a rearrangement must occur in order for 15 Fe^{3+}-PPIX equivalents to bind to an ordered structure. Formation of the disulfide bond is a step that could lock the two monomers into a specific orientation, but the C274S mutant has no apparent Fe^{3+}-PPIX binding deficiencies, suggesting that the disulfide is not a necessary step in Fe^{3+}-PPIX binding. Clearly, this is an area for future work in order to fully understand and confirm the complicated Fe^{3+}-PPIX binding model proposed here for HRP II.

CONCLUSION

The process of binding 15 Fe^{3+}-PPIX molecules requires HRP II to undergo large structural changes. Upon Fe^{3+}-PPIX binding, HRP II converts from a random coil to a structure with a CD spectrum suggestive of a 3_{10}-helix, a conformation commonly found in proteins but rarely longer than two turns. Along with these secondary structure changes there is a clear interaction between two HRP II monomers which is induced by Fe^{3+}-PPIX binding. This interaction is evident through both the pull-down assays performed and the Fe^{3+}-PPIX-dependent formation of an intermolecular disulfide.

The results suggest a model for Fe^{3+}-PPIX binding by HRP II, diagrammed in Figure 8, that is unique. Fe^{3+}-PPIX binding is able to bring about an interaction between two monomers, resulting in the formation of an intermolecular disulfide bond while also inducing a change in the secondary structure from a random coil to a 3_{10}-helix. The result of these structural changes is Fe^{3+}-PPIX bound between two HRP II helices by the aligned His residues, possibly leaving an exposed edge of Ala residues along the outside of the dimer.

ACKNOWLEDGMENT

We thank Dr. M. J. McLeish (University of Michigan) for help with the CD spectroscopy.

REFERENCES

1. WHO (2002) *World Health Organization Report on Infectious Diseases: Scaling up the Response to Infectious Diseases; A Way Out of Poverty*, World Health Organization, Geneva, Switzerland.
2. Meshnick, S. R. (1996) Is haemozoin a target for antimalarial drugs?, *Ann. Trop. Med. Parasitol. 90*, 367−372.
3. Goldberg, D. E., Slater, A. F., Cerami, A., and Henderson, G. B. (1990) Hemoglobin degradation in the malaria parasite *Plasmodium falciparum*: an ordered process in a unique organelle, *Proc. Natl. Acad. Sci. U.S.A. 87*, 2931−2935.
4. Rosenthal, P. J., and Meshnick, S. R. (1996) Hemoglobin catabolism and iron utilization by malaria parasites, *Mol. Biochem. Parasitol. 83*, 131−139.
5. Chou, A. C., and Fitch, C. D. (1981) Mechanism of hemolysis induced by ferriprotoporphyrin IX, *J. Clin. Invest. 68*, 672−677.
6. Fitch, C. D., Chevli, R., Banyal, H. S., Phillips, G., Pfaller, M. A., and Krogstad, D. J. (1982) Lysis of *Plasmodium falciparum* by ferriprotoporphyrin IX and a chloroquine-ferriprotoporphyrin IX complex, *Antimicrob. Agents Chemother. 21*, 819−822.
7. Pagola, S., Stephens, P. W., Bohle, D. S., Kosar, A. D., and Madsen, S. K. (2000) The structure of malaria pigment beta-haematin, *Nature 404*, 307−310.
8. Ursos, L. M., and Roepe, P. D. (2002) Chloroquine resistance in the malarial parasite, *Plasmodium falciparum*, *Med. Res. Rev. 22*, 465−491.
9. Sullivan, D. J. (2002) Theories on malarial pigment formation and quinoline action, *Int. J. Parasitol. 32*, 1645−1653.
10. Dorn, A., Stoffel, R., Matile, H., Bubendorf, A., and Ridley, R. G. (1995) Malarial haemozoin/beta-haematin supports haem polymerization in the absence of protein, *Nature 374*, 269−271.
11. Sullivan, D. J., Jr., Gluzman, I. Y., and Goldberg, D. E. (1996) *Plasmodium* hemozoin formation mediated by histidine-rich proteins, *Science 271*, 219−222.
12. Fitch, C. D., Cai, G. Z., Chen, Y. F., and Shoemaker, J. D. (1999) Involvement of lipids in ferriprotoporphyrin IX polymerization in malaria, *Biochim. Biophys. Acta 1454*, 31−37.
13. Bendrat, K., Berger, B. J., and Cerami, A. (1995) Haem polymerization in malaria, *Nature 378*, 138−139.
14. Pandey, A. V., Babbarwal, V. K., Okoyeh, J. N., Joshi, R. M., Puri, S. K., Singh, R. L., and Chauhan, V. S. (2003) Hemozoin formation in malaria: a two-step process involving histidine-rich proteins and lipids, *Biochem. Biophys. Res. Commun. 308*, 736−743.
15. Slater, A. F., and Cerami, A. (1992) Inhibition by chloroquine of a novel haem polymerase enzyme activity in malaria trophozoites, *Nature 355*, 167−169.
16. Choi, C. Y., Cerda, J. F., Chu, H. A., Babcock, G. T., and Marletta, M. A. (1999) Spectroscopic characterization of the heme-binding

sites in *Plasmodium falciparum* histidine-rich protein 2, *Biochemistry 38*, 16916−16924.
17. Akompong, T., Kadekoppala, M., Harrison, T., Oksman, A., Goldberg, D. E., Fujioka, H., Samuel, B. U., Sullivan, D., and Haldar, K. (2002) Trans expression of a *Plasmodium falciparum* histidine-rich protein II (HRPII) reveals sorting of soluble proteins in the periphery of the host erythrocyte and disrupts transport to the malarial food vacuole, *J. Biol. Chem. 277*, 28923−28933.
18. Wellems, T. E., and Howard, R. J. (1986) Homologous genes encode two distinct histidine-rich proteins in a cloned isolate of *Plasmodium falciparum*, *Proc. Natl. Acad. Sci. U.S.A. 83*, 6065−6069.
19. Panton, L. J., McPhie, P., Maloy, W. L., Wellems, T. E., Taylor, D. W., and Howard, R. J. (1989) Purification and partial characterization of an unusual protein of *Plasmodium falciparum*: histidine-rich protein II, *Mol. Biochem. Parasitol. 35*, 149−160.
20. Pandey, A. V., Bisht, H., Babbarwal, V. K., Srivastava, J., Pandey, K. C., and Chauhan, V. S. (2001) Mechanism of malarial haem detoxification inhibition by chloroquine, *Biochem. J. 355*, 333−338.
21. Morgan, W. T. (1985) The histidine-rich glycoprotein of serum has a domain rich in histidine, proline, and glycine that binds heme and metals, *Biochemistry 24*, 1496−1501.
22. Morgan, W. T. (1978) Human serum histidine-rich glycoprotein. I. Interactions with heme, metal ions and organic ligands, *Biochim. Biophys. Acta 535*, 319−333.
23. Gornall, A. G., Bardawill, C. J., and David, M. M. (1949) Determination of Serum Proteins by Means of the Biuret Reaction, *J. Biol. Chem. 177*, 751−766.
24. Toniolo, C., Polese, A., Formaggio, F., Crisma, M., and Kamphuis, J. (1996) Circular dichroism spectrum of a peptide 3(10)-helix, *J. Am. Chem. Soc. 118*, 2744−2745.
25. Greenfield, N., and Fasman, G. D. (1969) Computed circular dichroism spectra for the evaluation of protein conformation, *Biochemistry 8*, 4108−4116.
26. Andersen, N. H., Liu, Z., and Prickett, K. S. (1996) Efforts toward deriving the CD spectrum of a 3(10) helix in aqueous medium, *FEBS Lett. 399*, 47−52.
27. Lynn, A., Chandra, S., Malhotra, P., and Chauhan, V. S. (1999) Heme binding and polymerization by *Plasmodium falciparum* histidine rich protein II: influence of pH on activity and conformation, *FEBS Lett. 459*, 267−271.
28. Barlow, D. J., and Thornton, J. M. (1988) Helix geometry in proteins, *J. Mol. Biol. 201*, 601−619.
29. Bolin, K. A., and Millhauser, G. L. (1999) alpha and 3(10): The split personality of polypeptide helices, *Acc. Chem. Res. 32*, 1027−1033.
30. Karpen, M. E., de Haseth, P. L., and Neet, K. E. (1992) Differences in the amino acid distributions of 3(10)-helices and alpha-helices, *Protein Sci. 1*, 1333−1342.
31. Pal, L., and Basu, G. (1999) Novel protein structural motifs containing two-turn and longer 3(10)-helices, *Protein Eng. 12*, 811−814.
32. Biron, Z., Khare, S., Samson, A. O., Hayek, Y., Naider, F., and Anglister, J. (2002) A monomeric 3(10)-helix is formed in water by a 13-residue peptide representing the neutralizing determinant of HIV-1 on gp41, *Biochemistry 41*, 12687−12696.
33. Robertson, D. E., Farid, R. S., Moser, C. C., Urbauer, J. L., Mulholland, S. E., Pidikiti, R., Lear, J. D., Wand, A. J., DeGrado, W. F., and Dutton, P. L. (1994) Design and synthesis of multihaem proteins, *Nature 368*, 425−432.
34. Rosenblatt, M. M., Huffman, D. L., Wang, X., Remmer, H. A., and Suslick, K. S. (2002) Cyclic and hairpin peptide complexes of heme, *J. Am. Chem. Soc. 124*, 12394−12395.
35. Rosenblatt, M. M., Wang, J., and Suslick, K. S. (2003) De novo designed cyclic-peptide heme complexes, *Proc. Natl. Acad. Sci. U.S.A. 100*, 13140−13145.
36. Arnold, P. A., Shelton, W. R., and Benson, D. R. (1997) Peptide helix induction in a self-assembling hemoprotein model, *J. Am. Chem. Soc. 119*, 3181−3182.
37. Schneider, E. L., King, D. S., and Marletta, M. A. (2005) Amino acid substitution and modification resulting from *Escherichia coli* expression of recombinant *Plasmodium falciparum* histidine-rich protein II, *Biochemistry 44*, 987−995.

BI048570P